The Flow Around Surface-Mounted, Prismatic Obstacles Placed in a Fully Developed Channel Flow

(Data Bank Contribution*)

R. Martinuzzi

C. Tropea

Lehrstuhl für Strömungsmechanik,
Universität Erlangen-Nürnberg,
D-8520 Erlangen, Germany

The flow field around surface-mounted, prismatic obstacles with different spanwise dimensions was investigated using the crystal violet, oil-film and laser-sheet visualization techniques as well as by static pressure measurements. The aim of this study is to highlight the fundamental differences between nominally two-dimensional and fully three-dimensional obstacle flows. All experiments were performed in a fully developed channel flow. The Reynolds number, based on the height of the channel, lay between 8×10^4 and 1.2×10^5. Results show that the middle region of the wake is nominally two-dimensional for width-to-height ratios (W/H) greater than 6. The separated region in front of wider obstacles is characterized by the appearance of a quasi-regular distribution of saddle and nodal points on the forward face of the obstacles. These three-dimensional effects are considered to be inherent to such separating flows with stagnation.

1 Introduction

The study of the flow around surface-mounted, sharp-edged obstacles placed in a channel is fundamental to the understanding of the flow mechanisms for complex two- and three-dimensional geometries. There exists a considerable amount of published data for flows over two-dimensional geometries such as ribs and fences. However, there are markedly fewer studies in the literature concerned with the flow around three-dimensional obstacles. Of these, most are limited to the study of a single parameter, for example, the reattachment length. It is therefore the aim of this study to provide a general description of the flow around three-dimensional obstacles. Based on the flow visualization experiments performed for obstacles of different aspect ratio (width-to-height), the changes in the flow patterns as a function of aspect ratio are discussed qualitatively. Additionally, large-scale parameters such as the reattachment and separation lengths are discussed quantitatively.

The flow around single, surface-mounted, prismatic obstacles submerged in a boundary layer at high Reynolds numbers depends on a large number of parameters. Letting Ω denote a general function describing this flow field, the functional relationship to these parameters expressed in terms of non-dimensional groups is:

$$\Omega = f_1\left(\frac{\delta}{H'}\,\frac{u_\tau}{U_1'}\,\frac{l_w}{H'}\,\frac{W}{H'}\,\frac{L}{H'}\,\mathrm{Re}_H,\ \Lambda,\ \alpha\right)$$

where $\Lambda = l_f\sqrt{k_f}/U_1 H$ is the free-stream turbulence parameter.

Assuming that the boundary layer develops over a smooth wall, it can be shown that l_w, the length scale of the wall turbulence, is a direct and simple function of u_τ. Results of studies investigating these flows in terms of the parameters Hu_τ/ν, H/δ (Good and Joubert, 1968), HU_1/ν (Castro, 1979), δ/H (Castro and Robins, 1977) and of the free-stream turbulence parameter, Λ (Vincent, 1977, 1978) demonstrate that for a fixed obstacle geometry, these flows are mainly influenced by H, δ, Λ, and u_τ.

For the case of an obstacle placed in a fully developed channel flow, the number of parameters influencing the flow field is reduced. For this case, the boundary layer thickness is no longer relevant. The parameter Λ varies only to a small degree with the Reynolds number and the wall shear velocity (u_τ) changes slightly over a large range of Reynolds numbers (u_τ/U_1 varies about 20 percent between $\mathrm{Re} = 10^4$ and $\mathrm{Re} = 10^5$). Since the parameters defining the obstacle geometry are held constant, the flow can be considered to depend mainly on the parameters h/H and $\mathrm{Re}_H = U_B H/\nu$.

There is little published data on the flow around surface-mounted obstacles placed in a channel. Hence, the following general description of the flow field around surface-mounted, prismatic obstacles relies on data from investigations performed in boundary layer flows. The shape and form of the separation region over and behind the obstacle depends on the relative boundary layer thickness, δ/H. Whereas the form of the pressure distribution on the front face of a prismatic obstacle has been shown, for example, by Good and Joubert (1968) and Hunt (1982), to be insensitive to this parameter, the location of the separation point upstream of the obstacle is strongly dependent on δ/H. The separation point moves

*Data have been deposited to the JFE Data Bank. To access the file for this paper, see instructions on p. 189 of this issue.

Contributed by the Fluids Engineering Division for publication in the JOURNAL OF FLUIDS ENGINEERING. Manuscript received by the Fluids Engineering Division February 28, 1992. Associate Technical Editor: R. L. Panton.

closer to the obstacle with decreasing relative boundary-layer thickness. The slope of the separation streamline changes, which in turn determines the shape of the recirculation "bubble" downstream of the leading edge.

Up to four vortices have been observed to form in the region upstream of the wall-obstacle junction. This structure is similar to that observed for vertical, wall-mounted cylinders (Baker, 1980, 1991). These vortices extend over the entire width of the obstacle and are deflected downstream at its ends thereby forming the well-known horseshoe vortex system.

The mean flow reattaches on top of the three-dimensional obstacles at streamwise lengths much shorter than those of two-dimensional obstacles (Schofield and Logan, 1990). Moreover, the streamwise length of the obstacle for which reattachment occurs has been shown by Castro and Dianat (1984) to be a function of δ/H.

The recirculation region on top of the obstacle has been observed to consist of a multiple vortex system (see Castro and Robins, 1977; Woo et al., 1978) which gives rise to complicated surface shear stress patterns as shown by Dianat and Castro (1983) and Castro and Dianat (1984).

The flow around surface-mounted, three-dimensional obstacles is characterized by streamwise vortices generated within the shear layer. These vortices drastically affect the flow in the obstacle's vicinity, acting to reorganize the recirculation region and influence the downstream recovery region. As a result, the flow field for three-dimensional obstacle flows is intrinsically more complex than for the two-dimensional case.

Based on results obtained mainly from surface flow visualization techniques (Hunt et al., 1978; Perry and Hornung, 1984; and Fairlie, 1984), it has been shown that fluid is exchanged between the different separation regions formed around any three-dimensional obstacle. These regions are at the origin of line vortices which are shed into the downstream flow. It follows that the separation "bubble" formed around any surface-mounted, three-dimensional obstacle cannot be closed (Hunt et al., 1978).

Results from investigations performed by Logan and Lin (1982) and Fackrell and Pearce (1981) show that the separation length, x_R, and the recovery region downstream of the obstacle are much shorter for three-dimensional cases than for two-dimensional ones. This effect is probably due to the fact that the flow is mostly around, as opposed to over three-dimensional obstacles.

2 Experimental Apparatus and Techniques

The flows considered in this paper were investigated by means of static pressure measurements, laser light sheet, oil-film and crystal violet visualization techniques. The latter visualizations were performed in the water channel described by Ziegler (1987). A detailed description of this technique can be found in Dimaczek et al. (1988). The other experiments were performed in an open, blower-type air channel described in Larousse et al. (1991). The dimensions of the channel are 390 cm $\times$ 60 cm $\times$ 5 cm ($1 \times w \times h$). The leading edge of the obstacles was placed 52 channel heights downstream of the inlet. The boundary-layer was tripped at the inlet in order to obtain fully-developed conditions at least 5 channel heights upstream of the front face of the obstacles.

Pressure taps of 1.0 mm diameters were provided on the channel walls and the faces of the obstacles in order to perform static pressure measurements. These measurements were conducted using commercially available membrane-type pressure transducers (HBM) with a measuring range of ± 0.01 bar. The analogue transducer signal was sampled at frequencies of 100 Hz to 400 Hz and averaged for periods extending from 2 to 20 seconds.

A mixture of kerosene, light transmission oil and carbon powder (toner) was used for the oil-film visualizations. The results were preserved on black and white film.

The crystal violet experiments were conducted using a gentian violet based indicator solution deposited on fixed photographic paper which also served as a permanent record of the results.

The tracer particles for the laser light sheet visualization experiments were obtained using smoke from a commercially available fog-generator. The experiments were recorded with a video camera.

3 Experimental Results

Tests were conducted for Reynolds numbers based on the channel height, Re_h, ranging from 80,000 to 115,000. Prismatic obstacles with square cross-sections of various widths were mounted on the surface of the channel floor. The on-coming channel flow was determined to be fully developed (see Larousse et al., 1991).

The effect of the aspect ratio (W/H) on the flow patterns was investigated by performing visualization experiments. A cube and a rib spanning the entire width of the channel were chosen as representative cases for the fully three-dimensional and fully two-dimensional obstacle geometries respectively. Other obstacles with aspect ratios ranging between these were also investigated in order to study the transition between these two flow regimes. The geometric parameters for the different cases are summarized in Table 1. The geometry studied and the nomenclature used are summarized in Fig. 1.

The flow pattern for the two-dimensional rib obtained with the oil-film technique is shown in Fig. 2. With the exception of the corner effects due to the channel walls, the flow behind the obstacle is uniform. In this figure, line **A** corresponds to a clearly defined separation line upstream of the obstacle, while line **R** corresponds to the reattachment line.

On the front face of the obstacle, as can been from the crystal violet visualization results shown in Fig. 3, there is a series of alternating saddle and nodal points. This pattern can also be observed on the channel floor in the recirculation region

Nomenclature

B = blockage ratio ($= W \cdot H / w \cdot h$)
C_p = $(P - P_{\mathrm{atm}})/\frac{1}{2}\rho U_1^2$, pressure coefficient
ΔC_p = total pressure loss due to the obstacle
h,w,l = channel height, width and length
H,L,W = obstacle height, streamwise length, cross-stream width
W/H = obstacle aspect ratio
k_f = free-stream turbulence kinetic energy
Re_h = $U_B h/\nu$, Reynolds number based on the channel height
Re_H = $U_1 H/\nu$, Reynolds number based on the obstacle height
u,v,w = velocity components
U_1 = characteristic velocity
U_B = channel bulk velocity
u_τ = $\sqrt{\tau_w/\rho}$, wall shear velocity
x,y,z = streamwise, vertical and cross-stream coordinates
α = angle of attack
δ = boundary layer thickness
l_f = free-stream turbulent length scale
l_w = length scale of the wall turbulence
Λ = $l_f\sqrt{k_f}/U_1 H$, free stream turbulence parameter
ρ = fluid density
ν = fluid kinematic viscosity

Table 1 Summary of the obstacle geometries

H (cm)	H/h	W (cm)	W/H	H/W	H (cm)	H/h	W (cm)	W/H	H/W
2.50	0.50	2.50	1.00	1.000	2.50	0.50	25.0	10.0	0.100
2.50	0.50	5.00	2.00	0.500	2.50	0.50	35.0	14.0	0.071
2.50	0.50	10.0	4.00	0.250	2.50	0.50	50.0	20.0	0.050
2.50	0.50	12.5	5.00	0.200	2.50	0.50	55.0	22.0	0.045
2.50	0.50	15.0	6.00	0.167	2.50	0.50	60.0	24.0	0.041
2.50	0.50	20.0	8.00	0.125					

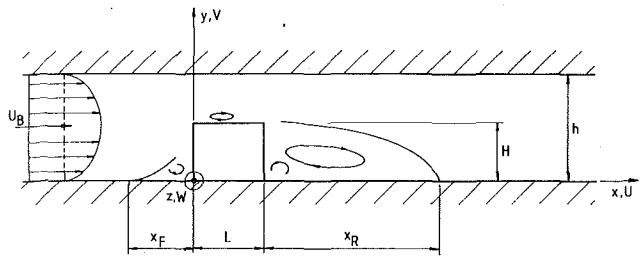

Fig. 1 Sketch of the obstacle geometry in a channel flow

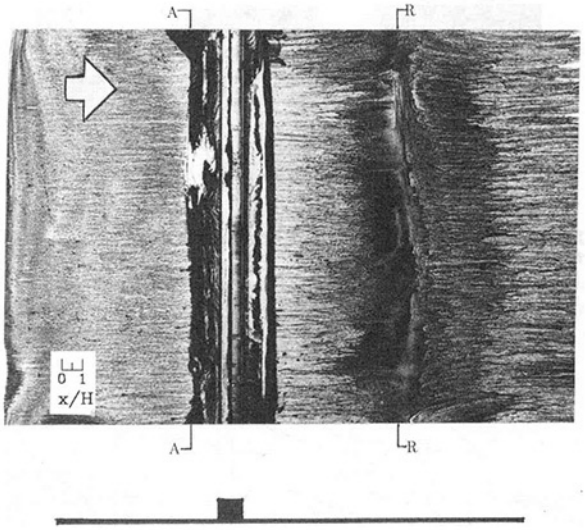

Fig. 2 Oil-film visualization results for a two-dimensional rib (Re_h = 10^5)

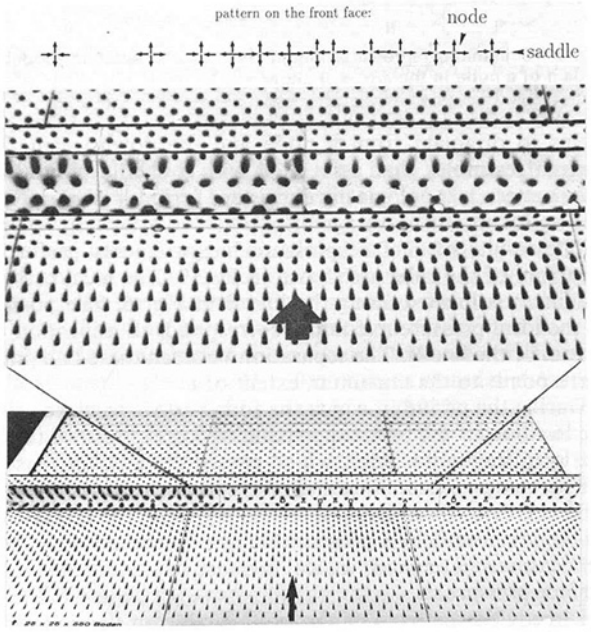

Fig. 3 Crystal violet results for a two-dimensional rib showing saddle and nodal points (Re_h = 10^5)

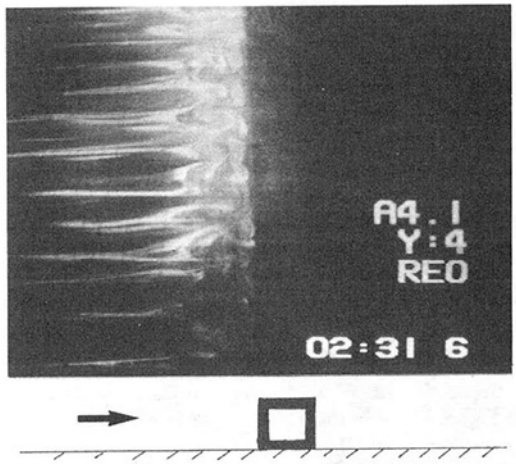

Fig. 4 Laser-sheet visualization of the flow over a two-dimensional rib (plane y/H = 0.16)

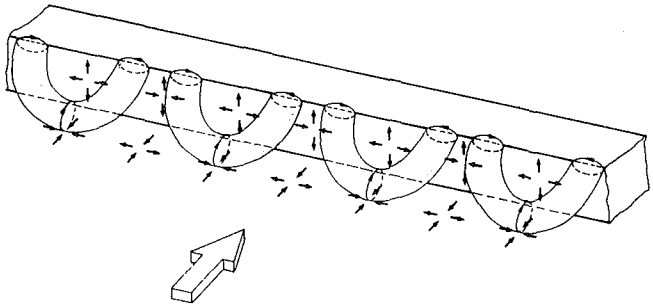

Fig. 5 Model of the flow on the upwind face of an obstacle

upstream of the obstacle. The location of these has been shown by Theisinger (1990) to be insensitive to small irregularities in the obstacle geometry. Further experiments performed using a laser light sheet technique show that the flow impinging on the front face of the obstacle does not preserve a two-dimensional character. Instead, the flow field develops a cellular structure, as can be seen in Fig. 4, which can still be recognized in the flow over the obstacle downstream of the leading edge. These three-dimensional structures suggest that the flow does not uniformly pass over the obstacle, but rather that this process occurs along preferred paths as is shown schematically in Fig. 5. Although highly idealized, this representation of the flow field is consistent with the observed surface patterns.

The results of the oil-film visualization for the flow around the cube are shown in Fig. 6(a) and Fig. 6(b). In these two figures, line **A** corresponds to the primary, upstream separation line and line **B** corresponds to the approximate time-averaged location of the center of the horseshoe vortex. Line **C** indicates a secondary recirculation at the front base of the cube.

As discussed by Larousse et al. (1991) and Devenport and Simpson (1990), the flow in the region between lines **A** and **B** is unstable and it is postulated that the fluid here is intermittently convected down to line **B**. The flow pattern seen adjacent to line **B** in Fig. 6(b) suggests however, a separation saddle point. This observation would only be topologically consistent

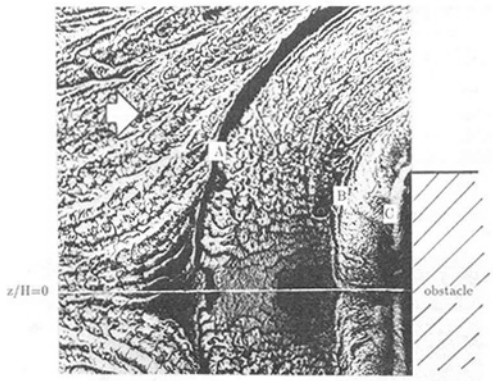

Fig. 6(*a*)

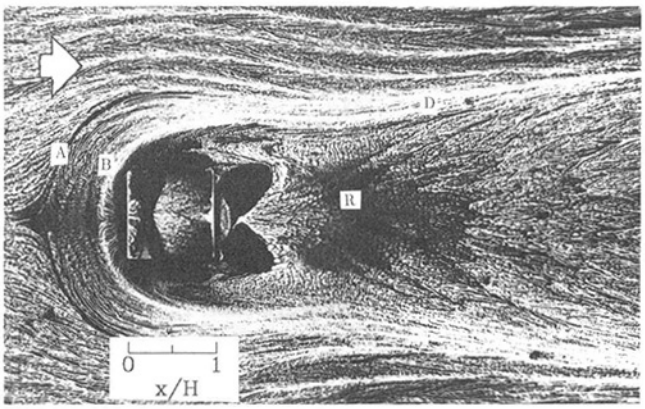

Fig. 6(*b*)

Fig. 6 Oil-film visualization results upstream of a surface-mounted cube

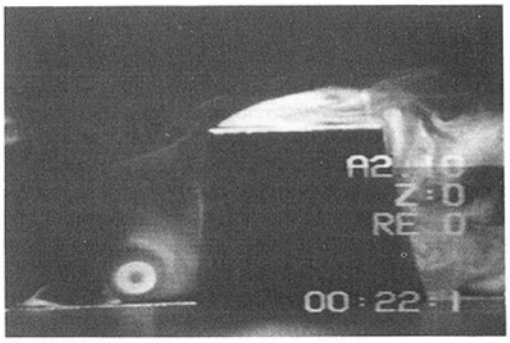

Fig. 7(*a*)

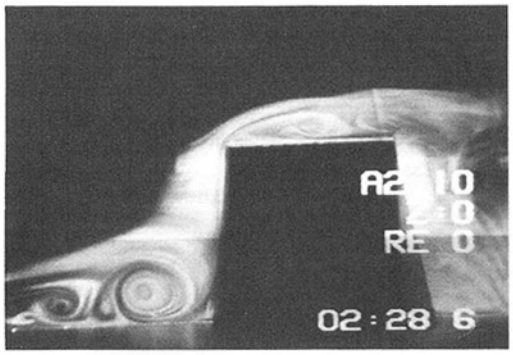

Fig. 7(*b*)

Fig. 7 Laser-sheet visualization of the flow in front of a cube (plane $z/H = 0$)

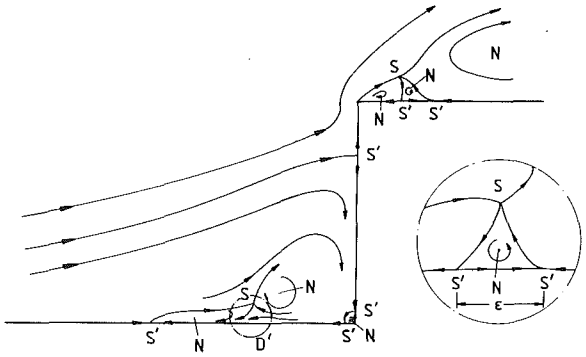

Fig. 8 Schematic representation of the mean-streamline model upstream of a cube in the $z/H = 0$ plane

if there were an additional reattachment node between lines **A** and **B** along the axis of symmetry. Such a node could not be observed in these visualization results. However, this pattern may be explained in one of two ways. First, the separation between the suspected reattachment node and the saddle point is smaller than can be resolved by either visualization technique. Such a flow pattern corresponds to that suggested by Hunt et al. (1978) and Baker (1980). A second possibility is, as suggested by Devenport and Simpson (1990) who also observed a similar pattern, that this pattern is due to an abrupt change in the magnitude of the shear stress along line **B**. It therefore does not correspond to a saddle point and the reverse flow adjacent to the channel floor is convected back to line **A**. A similar conclusion has been drawn by Eckerle and Awad (1991) based on time-averaged velocity measurements of the flow around a surface-mounted cylinder. It should be noted, however, that this interpretation is topologically inconsistent, since it violates Euler's criterium (see Hunt et al., 1978).

Pictures of the flow patterns in this region obtained from laser light sheet visualization experiments show that: In one mode, a jet adjacent to the wall can be observed (see Fig. 7(*a*)) which rolls up to form a series of vortices as is seen in Fig. 7(*b*)). Hence, it is postulated that the vortex structure suggested by Baker (1980) represents one of the two possible modes in this region. It follows that the two 'separation' lines observed in the oil-film visualization experiments correspond to the extent of the separation zone of one of the two modes, respectively. This latter explanation prompted the flow pattern proposed here in Fig. 8.

The point marked D' designates the location of a doublet which can be interpreted as a system consisting a free node, a reattachment and a separation half-saddle. The two half-saddle points are separated by a distance, ϵ, which has a time-averaged value of zero. Hence, the flow upstream of this point seems to originate from a node and the downstream flow pattern resembles that associated with a saddle point. This flow pattern is topologically consistent for both flow states as well as for the time-averaged flow.

The results of surface pressure measurements performed upstream of the cube are shown in Fig. 9. The local pressure minimum is located along the line **B** in Fig. 6. The position of the local pressure maximum corresponds to a location upstream of the line **B**. The separation between these two points corresponds to the maximum extent of ϵ.

During the period in which the four-vortex structure exists, the location of the pressure maximum corresponds to that of the local stagnation point which causes the local increase of the surface pressure. Since the relaxation time of the pressure field is greater than that of the velocity field, the imprint left on the pressure field is preserved long enough such that it can be measured in terms of a local increase of the time-averaged surface pressure.

Directly downstream of the leading edge on the side of the cube there is a corner vortex located at the junction of the channel floor and cube in addition to the horseshoe vortex,

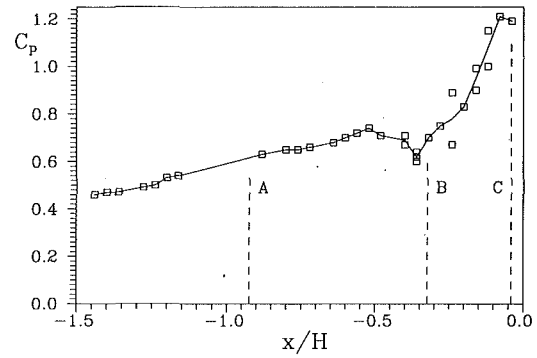

Fig. 9 *Cp* versus *x/H* along *z/H* = 0 in the region upstream of the cube ($Re_h = 10^5$). Uncertainty estimate on positioning, $\Delta x = \pm 0.5$ mm, $\Delta x/H = \pm 0.02$ and on pressure coefficient, $\Delta C_p = \pm 0.02$

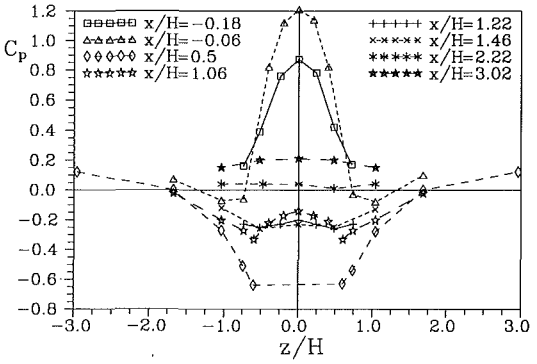

Fig. 10 *Cp* versus *z/H* for the flow around a cube ($Re_h = 10^5$). Uncertainty estimate on positioning, $\Delta x = \pm 0.2$ mm, $\Delta x/H = \pm 0.008$ and on pressure coefficient, $\Delta C_p = \pm 0.02$.

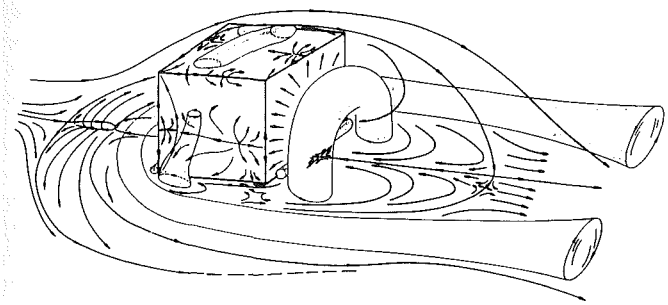

Fig. 11 Schematic representation of the flow around a surface-mounted cube

the imprint of which can be seen as local minima along the line for $x/H = 0.5$ in Fig. 10. From the visualizations, it was possible to determine that this vortex extends up the side along the lateral face of the cube and that it is fed along the floor-body junction by the corner vortex situated aft of the obstacle.

In Fig. 6(*a*), two corner vortices can be clearly seen behind the cube. The flow patterns observed on the leeward face of the obstacles suggest that the extension of these vortices join at the symmetry plane ($z/H = 0$) to form a closed arch behind the obstacle as suggested by Hunt et al. (1978).

The line **D** in Fig. 6(*a*) corresponds to the outer limits of the cube wake. The distance between the two ends of this line decreases up to approximately the reattachment point and then increases again. It is hereby postulated that directly behind the cube, the recirculation vortex entrains the surrounding fluid towards the axis of symmetry. After the reattachment point, the initially rapid expansion of the wake is due to the increase of the mass flux in the wake close to the channel floor as the shear layer reattaches and is subsequently entrained by the horseshoe vortex. Further downstream, the wake grows more

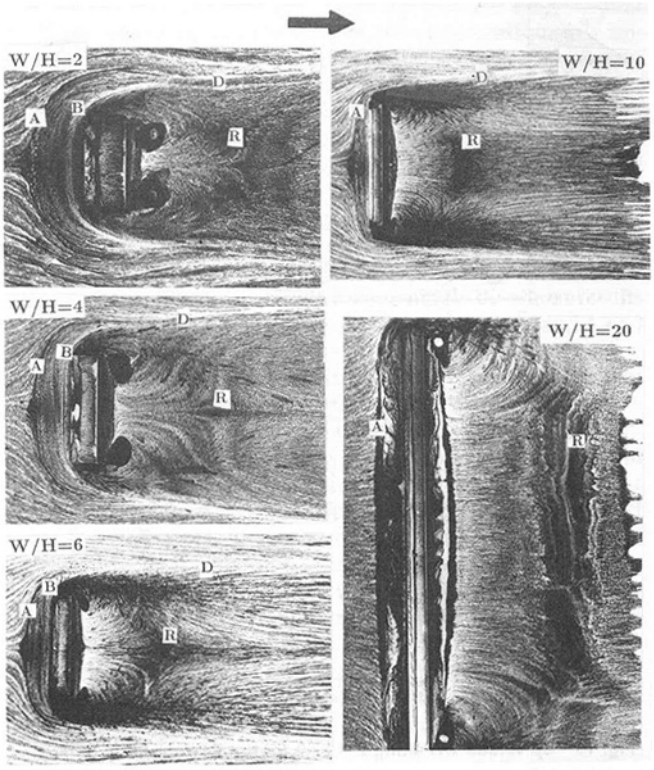

Fig. 12 An overview of oil-film visualization results for selected obstacles

slowly as fluid is gradually entrained from the surrounding flow. This flow pattern was observed for obstacles with aspect ratios of up to $W/H = 4$. The main features of the flow around small aspect ratio obstacles are summarized in schematic form in Fig. 11. This model was constructed with the aid of the results from the oil-film visualization experiments and those obtained from a detailed investigation of the velocity field around a cube (see Larousse et al., 1991).

An overview of the visualization results for selected geometries is shown in Fig. 12. Upstream of the obstacle, both the distance between lines **A** and **B** as well as the curvature of the separation line **A** decrease with increasing aspect ratio. For very large aspect ratios, only a single line of pigment accumulation can be recognized.

As reported by Devenport and Simpson (1990) and Larousse et al. (1991), the flow in the region between lines **A** and **B** is unsteady. Velocity measurements made by the latter authors and by Theisinger (1990) could not locate the characteristic velocity probability distribution associated with the bimodal-type instability for obstacles with aspect ratios greater than 10.

A clearly defined stagnation point can be seen on the front face of the obstacles with small aspect ratios. For aspect ratios greater than 10, an array of alternating saddle and node points similar to those for the two-dimensional rib (see Fig. 3) can be observed both on the front face and on the channel floor in the separated flow region.

The maximum and minimum pressures measured on the front and back of the obstacles, respectively, are lower for the three-dimensional cases than for the two-dimensional ones. The flow acceleration over the cube is weaker than over the rib which is consistent with this observation. Whereas the pressure recovery occurs rather quickly for small aspect ratios (see Fig. 13), the recovery region for the velocity field is significantly longer. Flow visualizations on the channel floor show significant mean cross-stream velocity components behind the cube for at least 20 heights downstream. The measured pressure coefficients shown in Fig. 10 clearly indicate the position of

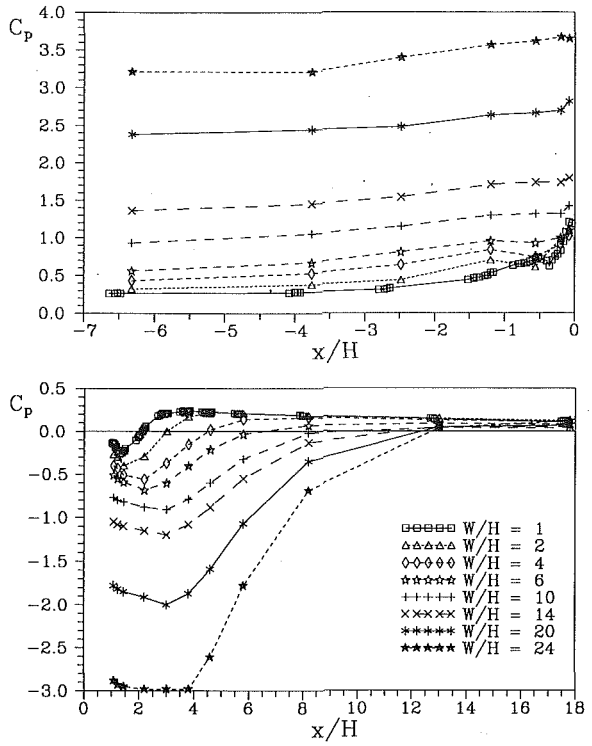

Fig. 13 *Cp* versus *x/H* along *z/H* = 0 for the flow around obstacles of varying *W/H* ($Re_h = 10^5$). Uncertainty estimate on positioning, $\Delta x = \pm 0.2$ mm, $\Delta x/H = \pm 0.008$ and on pressure coefficient, $\Delta C_p = \pm 0.02$.

the horseshoe vortex on the side of the obstacle (local minima for the curve $x/H = -0.06$) and the influence of the two corner vortices in the recirculating region (local minima for the curves $x/H = 1.06$ and 1.46).

For small aspect ratios, the visualization experiments show that the cross-channel velocity component, w, is non-zero in the wake. Pressure measurements indicate that the cross-channel pressure gradients in the wake are not negligible (see Fig. 10). The strongly three-dimensional nature of the wake is attributed to the influence of the streamwise oriented vorticity of the two ends of the horseshoe vortex. The relative separation of the two ends of the horseshoe vortex increases with the aspect ratio and there is a region of negligible w velocity about the $z/H = 0$ plane. The curvature of the reattachment line (marked **R** in Fig. 12) about the axis of symmetry is small for obstacles with aspect ratios greater than 6.

In the recirculation region, the orientation of the major axes and the location of the corner vortices change as a function of the aspect ratio. For small aspect ratios, the major axes of the elliptically shaped vortices are oriented away from the symmetry axis. For larger aspect ratios, these are oriented almost parallel to the obstacles. These changes are attributed to the effect of the pressure trough at the plane of symmetry which is stronger for longer obstacles.

The normalized leeward reattachment length (X_R/H) and windward separation length (X_F/H) are plotted as a function of the aspect ratio in Fig. 14. These show that on the back side of the obstacle, the reattachment length increases linearly with the obstacle width, W, up to about $W/H \approx 4$ and asymptotically approaches an end value of about 7.2. The location of the forward separation points appears to increase with W until $W/H \approx 6$ and then decreases slightly to a value of $X_F/H \approx 1.3$. However, because the effects of the blockage ratio, B, have not been explicitly investigated, it is difficult to draw further conclusions.

In all of the visualizations (see Figs. 2, 6, 12), except for the two-dimensional rib, the line **A** coincides with an accumulation of pigment associated with the presence of the separation zone

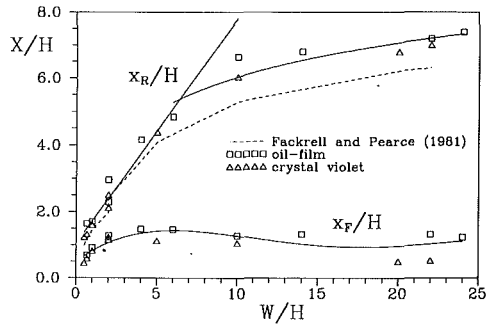

Fig. 14 Length of the upstream separation, X_F/H, and downstream reattachment, X_R/H, lengths as a function of *W/H* ($Re_h = 10^5$). Uncertainty estimate on crystal violet, $\Delta X_F = \pm 15$ percent ($W/H \leq 10$) and on oil-film, ± 5 percent; $\Delta X_F = \pm 60$ percent ($W/H > 14$) and on oil-film ± 7 percent; $\Delta X_R = \pm 3.5$ percent and on oil-film ± 5 percent

upstream of the obstacles. The pigment is transported to the sides by the deflected flow which extends this line around the forward corner of the obstacle.

Along the line **D**, which appears to be an extension of line **B**, there is a strong streamwise velocity component which rapidly transports pigment downstream leaving behind this white line. Line **D** effectively separates the wake from the flow to its sides. The flow in the wake is being convected away from the plane $z = 0$, while on the other side of this white line, the flow is predominantly in the streamwise direction. The change in the w velocity component occurs abruptly along this line.

4 Discussion

On the back and top sides of the obstacles, the appearance of a nominally two-dimensional region about the plane of symmetry can be recognized as soon as $W/H \approx 6$. The flow aft of the obstacle with small aspect ratio is dominated by the interaction of the horseshoe vortex with the recirculation vortex and the reattaching shear layer. For larger aspect ratios, the effect of the horseshoe vortex is predominantly observed along the edges of the wake. The inner portion of the wake is characterized by a small w velocity component and can be considered two-dimensional.

On the front of the obstacles, the appearance of a nominally two-dimensional region is characterized by a weak cross-channel velocity component, w, as well as with the appearance of an alternating saddle-nodal point arrangement typically found for the "2-D" rib on the front face of the obstacle. A two-dimensional region upstream of the separation line can be observed for W/H greater than 10.

The fact that the saddle-node array on the front-side of the obstacle appears at roughly the same aspect ratio for which the region of unsteady flow (located between the lines **A** and **B** in Fig. 12) can no longer be identified suggests that these two events are related. The evolution of the forward separating length, X_F/H, is consistent with this premise. For obstacles with a small aspect ratio, the on-coming flow is mostly deflected to the sides. For these small obstacles, the relative amount of fluid deflected increases proportionally with W/H. The size of the separation region, must, therefore, also increase. However, for larger obstacles, fluid accumulates in the recirculation region faster than it can flow around the sides. Hence, the fluid is increasingly forced over the obstacle. This mechanism explains the initial increase of X_F/H for small W/H and its near constant value for larger aspect ratios.

The process by which fluid is removed from the front of the obstacles is not uniform. As discussed in Simpson and Devenport (1990) and Larousse et al. (1991), the flow in the region between lines **A** and **B** is unsteady and oscillates between two preferred states. In one state, the recirculating region upstream of the obstacle is larger than that in the other, implying

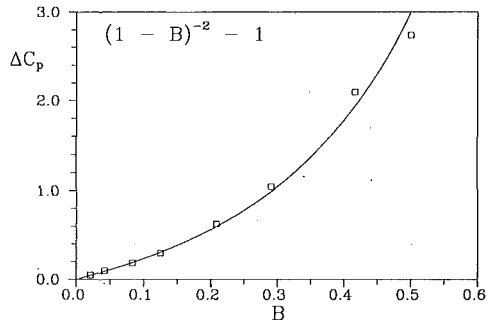

Fig. 15 Total pressure loss coefficient as a function of the blockage ratio, $B = W \cdot H/w \cdot h$ ($Re_h = 10^5$). Uncertainty estimate on pressure coefficient, $\Delta C_p = \pm 5$ percent for $W/H = 1$, based on 25 point curve and $\Delta C_p = \pm 9$ percent for $W/H > 2$ based on 6 point curve.

that the mass flux to the sides of the obstacle is irregular. This mechanism is considered to be typical for three-dimensional flows around obstacles with small aspect ratios.

As the aspect ratio increases, proportionally less fluid is channeled along the sides of the obstacles and correspondingly more must flow over the top. As this occurs, a distinct, quasi-equidistant array of alternating node and saddle points becomes evident. These suggest that the flow over the obstacle follows preferred paths and that this feature is an inherent characteristic of separating flows with stagnation for large aspect ratios. It follows then that the flow is always locally three-dimensional even in the case of the two-dimensional rib.

In view of this interpretation, it is to be expected that the blockage ratio is an important parameter in determining the total pressure loss in the channel. As can be seen in Fig. 15, the total pressure loss due to the obstacle, expressed as a loss coefficient, ΔC_p, is related to the blockage ratio, B, by the expression:

$$\Delta C_p = \frac{1}{(1-B)^2} - 1$$

which is obtained by assuming that the entire gain in kinetic energy at the obstacle plane is dissipated downstream. The expression for the average gain in kinetic energy was derived from the Bernoulli and continuity equations. In order to experimentally determine ΔC_p, the pressure difference between two locations, one far upstream and the other far downstream of the obstacle, was measured. The pressure difference between the same two locations was then measured for the same Reynolds number with the obstacle removed. The difference between these two values represents the loss due to the presence of the obstacle and, when normalized with $\frac{1}{2}\rho U_B^2$, yields ΔC_p.

For three-dimensional flows, there is typically an additional thin separation region in front of the horseshoe vortex adjacent to the wall where strong, adverse pressure gradients dominate. The presence of a free-stream stagnation saddle point in this region, which can be seen in Fig. 8, indicates that this region is not a part of the horseshoe vortex and that no vortex is present in this region in this plane. This view subscribes to those offered by Eckerle and Awad (1991) as well as Devenport and Simpson (1990).

5 Conclusions

The flow around obstacles of different aspect ratios (W/H) was investigated. It has been shown that a nominally two-dimensional region exists behind the obstacle for $W/H > 6$ and upstream of the recirculation region in front of the obstacles for $W/H > 10$. Typically for such obstacles, the recirculation region on the upstream side is inherently three-dimensional. It is characterized by the appearance of a nearly equally spaced array of alternating saddle and node points on the front face of the obstacles. This observation suggests that for large aspect ratios, the flow in the recirculation area upstream of the obstacle develops a cellular structure and passes over the obstacle along preferred paths.

For obstacles of small aspect ratio, the separation region upstream of the obstacles is characterized as alternating between two states. In one mode, high-inertia fluid is deflected on the front face of the obstacle back upstream in a jet adjacent to the wall. This fluid moves against the pressure gradient. As the fluid loses energy, it rolls up to form a system of up to four vortices. This structure characterizes the second mode. This mechanism helps reconcile the seemingly divergent results obtained by Baker (1980, 1991) with those by Eckerle and Awad (1991).

Pressure measurements and visualization results indicate that the recovery length behind a three dimensional obstacle is shorter than in the case of a two-dimensional flow. The interaction of the horseshoe vortex with the corner vortex behind the cube and with the impinging mixing-layer in the wake dominates the flow structure for obstacle with small aspect ratios ($W/H < 4$). It has also been shown that the total pressure loss is a function of the blockage ratio.

As the aspect ratio increases, the two ends of the horseshoe vortex are farther apart and have a smaller influence on the middle region of the wake. For larger aspect ratios, the w velocity component and the pressure gradient in the cross-channel direction in the middle of the wake are negligible. This region can therefore be treated as nominally two-dimensional.

JFE Data Bank Contributions

The experimental data obtained for the cube obstacle have been added to the *Journal of Fluids Engineering* Data Bank. These data include the three components of the mean velocity and all Reynolds stress components at numerous upstream and downstream positions. To access the file for this paper, see instructions on page 189 of this issue.

Acknowledgment

This work was financially supported by the Deutsche Forschungsgemeinschaft under contract TR 194/3.

References

Baker, C. J., 1980, "The Turbulent Horseshoe Vortex," *Journal of Wind Engineering and Industrial Aerodynamics*, Vol. 6, pp. 9-23.

Baker, C. J., 1991, "The Oscillation of Horseshoe Vortex System," ASME JOURNAL OF FLUIDS ENGINEERING, Vol. 113, pp. 489-495.

de Brederode, V., and Bradshaw, P., 1972, "Three-Dimensional Flow in Nominally Two-Dimensional Separation Bubbles I: Flow Behind a Rearward-Facing Step," IC Aero Report, 72-19, Imperial College, London.

Castro, I. P., and Robins, A. G., 1977, "The Flow Around a Surface-Mounted Cube in Uniform and Turbulent Streams," *Journal of Fluid Mechanics*, Vol. 79, part 2, pp. 307-335.

Castro, I. P., 1979, "Relaxing Wakes Behind Surface-Mounted Obstacles in Rough Wall Boundary Layers," *Journal of Fluid Mechanics*, Vol. 93, part 4, pp. 631-659.

Castro, I. P., and Dianat, M,. 1984, "Surface Flow Patterns on Rectangular Bodies in Thick Boundary Layers," *Journal of Wind Engineering and Industrial Aerodynamics*, Vol. 11, pp. 107-119.

Devenport, W. J., and Simpson, R. L., 1990, "Time-Dependent and Time-Averaged Turbulence Structure Near the Nose of a Wing-Body Junction," *Journal of Fluid Mechanics*, Vol. 210, pp. 23-55.

Dianat, M., and Castro, I. P., 1983, "Fluctuating Surface Shear Stresses on Bluff Bodies," *Journal of Wind Engineering and Industrial Aerodynamics*, Vol. 17, pp. 133-146.

Dimaczek, G., Eh, C., and Tropea, C., 1988, "Sichtbarmachung von Wasserströmungen mit Hilfe des Kristalviolettverfahrens," DLGR Workshop 2D-Meatechnik, Marktdorf, DLGR-Bericht 88-04.

Dimaczek, G., Kessler, R., Martinuzzi, R, and Tropea, C., 1989, "The Flow Over Two-Dimensional, Surface-Mounted Obstacles at High Reynolds Numbers," *Proc. 7th Symposium on Turbulent Shear Flows*, Standford, CA.

Eckerle, W. A., and Awad, J. K., 1991, "Effect of Freestream Velocity on the Three-Dimensional Separated Flow Region in Front of a Cylinder," ASME JOURNAL OF FLUIDS ENGINEERING, Vol. 113, pp. 37-44.

Fackrell, J. E., and Pearce, J. E., 1981, "Parameters Affecting Dispersion in the Near Wake of Buildings," CEGB Report No. RD/M/1179/N81.

Good, M. C., and Joubert, P. N., 1986, "The Form Drag of Two-Dimensional Bluff-Plates Immersed in Turbulent Boundary Layers," *Journal of Fluid Mechanics*, Vol. 31, pp. 547–582.

Hunt, J. C. R., Abell, C. J., Peterka, J. A., and Woo, H., 1978, "Kinematical Studies of the Flows Around Free or Surface- Mounted Obstacles, Applying Topology to Flow Visualization," *Journal of Fluid Mechanics*, Vol. 86, pp. 179–200.

Hunt, A., 1982, "Wind-Tunnel Measurements of Surface Pressure on Cube Building Models at Several Scales," *Journal of Wind Engineering and Industrial Aerodynamics*, Vol. 10, pp. 137–163.

Hussain, A. K. M. F., and Reynolds, W. C., 1975, "Measurements in Fully Developed Turbulent Channel Flow," ASME JOURNAL OF FLUIDS ENGINEERING, Dec. pp. 568–579.

Larousse, A., Martinuzzi, R., and Tropea, C., 1991, "Flow Around Surface-Mounted, Three-Dimensional Obstacles," *Proceedings 8th Symposium on Turbulent Shear Flows*, Munich, FRG.

Logan, E., and Lin, S. H., 1982, "Wakes from Arrays of Buildings," NASA Cr-170666.

Moore, J., and Forlini, T. J., 1984, "A Horseshoe Vortex in a Duct," ASME *Journal of Engineering for Gas Turbines and Power*, Vol. 106, pp. 668–675.

Schofield, W. H., and Logan, E., 1990, "Turbulent Shear Flow Over Surface-Mounted Obstacles," ASME JOURNAL OF FLUIDS ENGINEERING, Vol. 112, pp. 376–385.

Theisinger, J., 1990, "Untersuchung der Dreidimensionalität einer Rippenströmung im Flachkanal mittels LDA," Diplomarbeit, at the Lehrstuhl für Strömungsmechanik of the University Erlangen-Nuremberg.

Vincent, J. H., 1977, "Model Experiments on the Nature of Air Pollution Transport Near Buildings," *Atmospheric Environments*, Vol. 11, pp. 765–774.

Vincent, J. H., 1978, "Scalar Transport in the Near Aerodynamic Wakes of Surface-Mounted Cubes," *Atmospheric Environments*, Vol. 12, pp. 1319–1322.

Woo, H. G. C., Peterka, J., and Cermak, J. E. 1976, "Wind Tunnel Measurements in Wakes of Structures," Colorado State Univ. Rept. CER7575-76 HGWC-JAP-JEC40.

Ziegler, T., 1987, "Experimentelle Untersuchungen der Strömung über ein zweidimensionales Hindernis," Diplomarbeit at the Lehrstuhl für Strömungsmechanik of the University Erlangen-Nuremberg.